Title	Ultrahigh-Q photonic crystal nanocavities fabricated by CMOS process technologies
Author(s)	Ashida, Kohei; Okano, Makoto; Ohtsuka, Minoru; Seki, Miyoshi; Yokoyama, Nobuyuki; Koshino, Keiji; Mori, Masahiko; Asano, Takashi; Noda, Susumu; Takahashi, Yasushi
Editor(s)	
Citation	Optics Express. 2017, 25 (15), p.18165-18174
Issue Date	2017-07-24
URL	http://hdl.handle.net/10466/15720
Rights	(c) 2017 Optical Society of America. Users may use, reuse, and build up on the article, or use the article for text or data mining, so long as such uses are for non-commercial purposes and appropriate attribution is maintained. All other rights are reserved.

Research Article | Vol. 25, No. 15 | 24 Jul 2017 | OPTICS EXPRESS 18165
Optics EXPRESS

Ultrahigh-*Q* photonic crystal nanocavities fabricated by CMOS process technologies

KOHEI ASHIDA,[1] MAKOTO OKANO,[2,5] MINORU OHTSUKA,[2] MIYOSHI SEKI,[2] NOBUYUKI YOKOYAMA,[2] KEIJI KOSHINO,[2] MASAHIKO MORI,[2] TAKASHI ASANO,[3] SUSUMU NODA,[3,4] AND YASUSHI TAKAHASHI[1,*]

[1]*Department of Physics and Electronics, Osaka Prefecture University, Sakai, Osaka 599-8570, Japan*
[2]*National Institute of Advanced Industrial Science and Technology, Tsukuba, Ibaraki 305-8569, Japan*
[3]*Department of Electronic Science and Engineering, Kyoto University, Kyoto 615-8510 Japan*
[4]*Photonics and Electronics Science and Engineering Center, Kyoto University, Kyoto 615-8510 Japan*
[5]*makoto-okano@aist.go.jp*
**y-takahashi@pe.osakafu-u.ac.jp*

Abstract: We fabricated photonic crystal high-quality factor (*Q*) nanocavities on a 300-mm-wide silicon-on-insulator wafer by using argon fluoride immersion photolithography. The heterostructure nanocavities showed an average experimental *Q* value of 1.5 million for 12 measured samples. The highest *Q* value was 2.3 million, which represents a record for a nanocavity fabricated by complementary metal–oxide–semiconductor (CMOS)-compatible machinery. We also demonstrated an eight-channel drop filter with 4 nm spacing consisting of arrayed nanocavities with three missing air holes. The standard deviation in the drop wavelength was less than 1 nm. These results will accelerate ultrahigh-*Q* nanocavity research in various areas.

OCIS codes: (230.5298) Photonic crystals; (220.3740) Lithography; (220.4610) Optical fabrication; (230.5750) Resonators; (140.3948) Microcavity devices.

References and links

1. S. Noda, A. Chutinan, and M. Imada, "Trapping and emission of photons by a single defect in a photonic bandgap structure," Nature **407**(6804), 608–610 (2000).
2. Y. Akahane, T. Asano, B. S. Song, and S. Noda, "High-*Q* photonic nanocavity in a two-dimensional photonic crystal," Nature **425**(6961), 944–947 (2003).
3. B. S. Song, S. Noda, T. Asano, and Y. Akahane, "Ultra-High-*Q* photonic double-heterostructure nanocavity," Nat. Mater. **4**(3), 207–210 (2005).
4. D. Englund, I. Fushman, and J. Vučković, "General recipe for designing photonic crystal cavities," Opt. Express **13**(16), 5961–5975 (2005).
5. E. Kuramochi, M. Notomi, S. Mitsugi, A. Shinya, T. Tanabe, and T. Watanabe, "Ultrahigh-*Q* photonic crystal nanocavities realized by the local width modulation of a line defect," Appl. Phys. Lett. **88**(4), 041112 (2006).
6. E. Kuramochi, H. Taniyama, T. Tanabe, A. Shinya, and M. Notomi, "Ultrahigh-*Q* two-dimensional photonic crystal slab nanocavities in very thin barriers," Appl. Phys. Lett. **93**(11), 111112 (2008).
7. Y. Lai, S. Pirotta, G. Urbinati, D. Gerace, M. Minkov, V. Savona, A. Badolato, and M. Galli, "Genetically designed L3 photonic crystal nanocavities with measured quality factor exceeding one million," Appl. Phys. Lett. **104**(24), 241101 (2014).
8. T. Nakamura, Y. Takahashi, Y. Tanaka, T. Asano, and S. Noda, "Improvement in the quality factors for photonic crystal nanocavities via visualization of the leaky components," Opt. Express **24**(9), 9541–9549 (2016).
9. Y. Takahashi, Y. Tanaka, H. Hagino, T. Sugiya, Y. Sato, T. Asano, and S. Noda, "Design and demonstration of high-Q photonic heterostructure nanocavities suitable for integration," Opt. Express **17**(20), 18093–18102 (2009).
10. Y. Taguchi, Y. Takahashi, Y. Sato, T. Asano, and S. Noda, "Statistical studies of photonic heterostructure nanocavities with an average Q factor of three million," Opt. Express **19**(12), 11916–11921 (2011).
11. R. Terawaki, Y. Takahashi, M. Chihara, Y. Inui, and S. Noda, "Ultrahigh-*Q* photonic crystal nanocavities in wide optical telecommunication bands," Opt. Express **20**(20), 22743–22752 (2012).
12. H. Sekoguchi, Y. Takahashi, T. Asano, and S. Noda, "Photonic crystal nanocavity with a *Q*-factor of ~9 million," Opt. Express **22**(1), 916–924 (2014).
13. K. Maeno, Y. Takahashi, T. Nakamura, T. Asano, and S. Noda, "Analysis of high-*Q* photonic crystal L3 nanocavities designed by visualization of the leaky components," Opt. Express **25**(1), 367–376 (2017).

#296728 https://doi.org/10.1364/OE.25.018165
Journal © 2017 Received 29 May 2017; revised 14 Jul 2017; accepted 17 Jul 2017; published 19 Jul 2017

Optics EXPRESS

14. T. Asano, Y. Ochi, Y. Takahashi, K. Kishimoto, and S. Noda, "Photonic crystal nanocavity with a Q factor exceeding eleven million," Opt. Express **25**(3), 1769–1777 (2017).
15. Y. Takahashi, T. Asano, D. Yamashita, and S. Noda, "Ultra-compact 32-channel drop filter with 100 GHz spacing," Opt. Express **22**(4), 4692–4698 (2014).
16. M. G. Scullion, T. F. Krauss, and A. Di Falco, "Slotted photonic crystal sensors," Sensors (Basel) **13**(3), 3675–3710 (2013).
17. S. Iwamoto, Y. Arakawa, and A. Gomyo, "Observation of enhanced photoluminescence from silicon photonic crystal nanocavity at room temperature," Appl. Phys. Lett. **91**(21), 211104 (2007).
18. T. Ihara, Y. Takahashi, S. Noda, and Y. Kanemitsu, "Enhanced radiative recombination rate for electron-hole droplets in silicon photonic crystal nanocavity," under submission.
19. Y. Tanaka, J. Upham, T. Nagashima, T. Sugiya, T. Asano, and S. Noda, "Dynamic control of the Q factor in a photonic crystal nanocavity," Nat. Mater. **6**(11), 862–865 (2007).
20. Y. Sato, Y. Tanaka, J. Upham, Y. Takahashi, T. Asano, and S. Noda, "Strong coupling between distant photonic nanocavities and its dynamic control," Nat. Photonics **6**(1), 56–61 (2012).
21. R. Konoike, H. Nakagawa, M. Nakadai, T. Asano, Y. Tanaka, and S. Noda, "On-demand transfer of trapped photons on a chip," Sci. Adv. **2**(5), e1501690 (2016).
22. T. Tanabe, H. Sumikura, H. Taniyama, A. Shinya, and M. Notomi, "All-silicon sub-Gb/s telecom detector with low dark current and high quantum efficiency on chip," Appl. Phys. Lett. **96**(10), 101103 (2010).
23. Y. Takahashi, Y. Inui, M. Chihara, T. Asano, R. Terawaki, and S. Noda, "A micrometre-scale Raman silicon laser with a microwatt threshold," Nature **498**(7455), 470–474 (2013).
24. Y. Takahashi, Y. Inui, M. Chihara, T. Asano, R. Terawaki, and S. Noda, "High-*Q* resonant modes in a photonic crystal heterostructure nanocavity and applicability to a Raman silicon laser," Phys. Rev. B **88**(23), 235313 (2013).
25. T. Asano, B. S. Song, and S. Noda, "Analysis of the experimental *Q* factors (~ 1 million) of photonic crystal nanocavities," Opt. Express **14**(5), 1996–2002 (2006).
26. H. Hagino, Y. Takahashi, Y. Tanaka, T. Asano, and S. Noda, "Effects of fluctuation in air hole radii and positions on optical characteristics in photonic crystal heterostructure nanocavities," Phys. Rev. B **79**(8), 085112 (2009).
27. H. C. Nguyen, N. Yazawa, S. Hashimoto, S. Otsuka, and T. Baba, "Sub-100μm Photonic Crystal Si Optical Modulators: Spectral, Athermal, and High-Speed Performance," IEEE J. Sel. Top. Quantum Electron. **19**(6), 127–137 (2013).
28. Y. Ooka, T. Tetsumoto, A. Fushimi, W. Yoshiki, and T. Tanabe, "CMOS compatible high-*Q* photonic crystal nanocavity fabricated with photolithography on silicon photonic platform," Sci. Rep. **5**(1), 11312 (2015).
29. W. Xie, M. Fiers, S. Selvaraja, P. Bienstman, J. V. Campenhout, P. Absil, and D. V. Thourhout, "High-*Q* Photonic Crystal Nanocavities on 300mm SOI Substrate Fabricated With 193 nm Immersion Lithography," J. Lightwave Technol. **32**(8), 1457–1462 (2014).
30. D. P. Sanders, "Advances in patterning materials for 193 nm immersion lithography," Chem. Rev. **110**(1), 321–360 (2010).
31. T. Terasawa, N. Hasegawa, H. Fukuda, and S. Katagiri, "Imaging characteristics of multi-phase-shifting and halftone phase-shifting masks," Jpn. J. Appl. Phys. **30**(1), 2991–2997 (1991).
32. J. Lu, L. Zhang, H. Takagi, and R. Maeda, "A novel cavity-first process for flexible fabrication of MEMS on silicon on insulator (SOI) wafer," Microelectron. Eng. **119**(1), 28–31 (2014).
33. M. M. Torunbalci, S. E. Alper, and T. Akin, "Advanced MEMS Process for Wafer Level Hermetic Encapsulation of MEMS Devices Using SOI Cap Wafers With Vertical Feedthroughs," J. Microelectromech. Syst. **24**(3), 556–564 (2015).
34. A. Chutinan, M. Mochizuki, M. Imada, and S. Noda, "Surface-emitting channel drop filters using single defects in two-dimensional photonic crystal slabs," Appl. Phys. Lett. **79**(17), 2690–2692 (2001).
35. Q. Fang, T. Y. Liow, J. F. Song, K. W. Ang, M. B. Yu, G. Q. Lo, and D. L. Kwong, "WDM multi-channel silicon photonic receiver with 320 Gbps data transmission capability," Opt. Express **18**(5), 5106–5113 (2010).
36. Q. Fang, Y. T. Phang, C. W. Tan, T. Y. Liow, M. B. Yu, G. Q. Lo, and D. L. Kwong, "Multi-channel silicon photonic receiver based on ring-resonators," Opt. Express **18**(13), 13510–13515 (2010).
37. Y. Ooka, T. Tetsumoto, N. A. B. Daud, and T. Tanabe, "Ultrasmall in-plane photonic crystal demultiplexers fabricated with photolithography," Opt. Express **25**(2), 1521–1528 (2017).
38. Y. Akahane, T. Asano, H. Takano, B. S. Song, Y. Takana, and S. Noda, "Two-dimensional photonic-crystal-slab channeldrop filter with flat-top response," Opt. Express **13**(7), 2512–2530 (2005).

1. Introduction

Nanocavities based on artificial defects in two-dimensional (2D) photonic crystal (PC) slabs have a high-quality factor (Q) with a small modal volume (V) approaching one cubic wavelength [1–8]. In particular, nanocavities fabricated on a silicon-on-insulator (SOI) wafer have achieved the highest experimental Q (Q_{exp}) exceeding several million [9–14]. A high Q/V ratio brings many benefits; therefore, silicon (Si) high-Q nanocavities are being widely studied in various fields. Nanocavities with Q_{exp} of less than several hundred thousand have

been used in research on ultrasmall wavelength-selective filters [15], highly sensitive biosensors [16], and highly efficient Si emitters [17, 18]; these mainly utilize nanocavities with three missing air holes (L3) [2]. Heterostructure nanocavities with Q_{exp} of greater than several hundred thousand have helped realize unique devices such as an optical pulse trap with dynamic control [19–21] and two photon absorption photodiodes with low operating energies [22]. Ultrahigh-Q nanocavities with Q_{exp} of greater than 1 million have helped realize ultralow-threshold Raman Si lasers [23, 24]. In most of these studies, the nanocavities were fabricated with electron-beam (EB) lithography.

Heterostructure nanocavities can be designed with a theoretical Q (Q_{ideal}) value of greater than 10 million [3]. However, Q_{exp} is easily reduced to less than 1 million by nanometer-scale random variations in PC structures. Previous studies have clarified that fluctuations in the radii and positions of the air holes should be reduced to less than 1 nm in order to fabricate ultrahigh-Q nanocavities with Q_{exp} of greater than 1 million [25, 26]. High accuracy and high resolution are inevitably required for the lithography process, so EB lithography has been utilized. The EB machine has another merit in that the lithography pattern can easily be changed. However, the EB process requires a long time for lithography. Our research group has fabricated nanocavities on a small SOI chip with an area of about 1 cm^2.

Recently, the mass-manufacturing of Si PC functional devices utilizing a complementary metal–oxide–semiconductor (CMOS)-compatible process with photolithography has attracted attention. Following research on a high-speed optical modulator using a slow-light PC waveguide [27], a Q_{exp} value of 0.22 million was reported for glass-clad 2D PC nanocavities fabricated with krypton fluoride lithography [28], and a Q_{exp} value of 0.11 million was reported for 1D PC nanocavities fabricated with argon fluoride (ArF) immersion lithography [29]. However, ultrahigh-Q nanocavities with Q_{exp} of greater than several million have not been achieved with the CMOS fabrication process, which would be a significant step toward the commercial application of ultrahigh-Q nanocavities.

In this study, we fabricated high-Q nanocavities on a 300-mm SOI wafer using CMOS technologies. We used ArF immersion lithography with a half-tone mask and process recipe optimized for PC devices. An average Q_{exp} value of 1.5 million was obtained for 12 measured heterostructure nanocavities, where the highest value was 2.2 million. We also estimated the magnitude of random air hole variations for the measured sample to be 0.79 nm by comparing the Q_{exp} values with the calculated values. We demonstrated eight-channel drop filters with 4 nm spacing consisting of arrayed L3 nanocavities. The best sample showed a standard deviation of less than 0.5 nm for the drop wavelength.

2. Sample structure and fabrication process

Figures 1(a) and 1(b) show a schematic illustration and scanning electron microscopy (SEM) image, respectively, of a measured heterostructure nanocavity. We used a commercial 300-mm-wide SOI wafer with a 225-nm-thick Si slab and buried oxide (BOX) layer with a thickness of 2 μm. The PC consisted of a triangular lattice of circular air holes with radii of 105 nm. The nanocavity was formed by a line defect of 23 missing air holes. The lattice constant in the x-direction changed by 5 nm every two periods as it approached the center of the cavity. The lattice constants of the central, intermediate and outer regions were a_3 = 420 nm, a_2 = 415 nm, and a_1 = 410 nm, respectively, while the lattice constant in the y-direction was 710 nm (W_1) for all regions. The excitation waveguide adjacent to the cavity was 10% wider in the y-direction (i.e., 1.1W_1), and the separation from the cavity was eight rows of air holes. No special structure to improve the coupling efficiency to the waveguide was introduced at the waveguide edge. The calculated Q_{ideal} and resonant wavelength (λ_0) using the three-dimensional (3D) finite difference time domain (FDTD) method were 2.1×10^7 and 1605.8 nm, respectively. The fundamental structure of the nanocavity was the same as that for previous studies reporting Q_{exp} of several million fabricated with EB lithography [10–12].

The Q_{ideal} value in this study is slightly larger than those for our previous papers because of the smaller air hole radius [9, 10, 26].

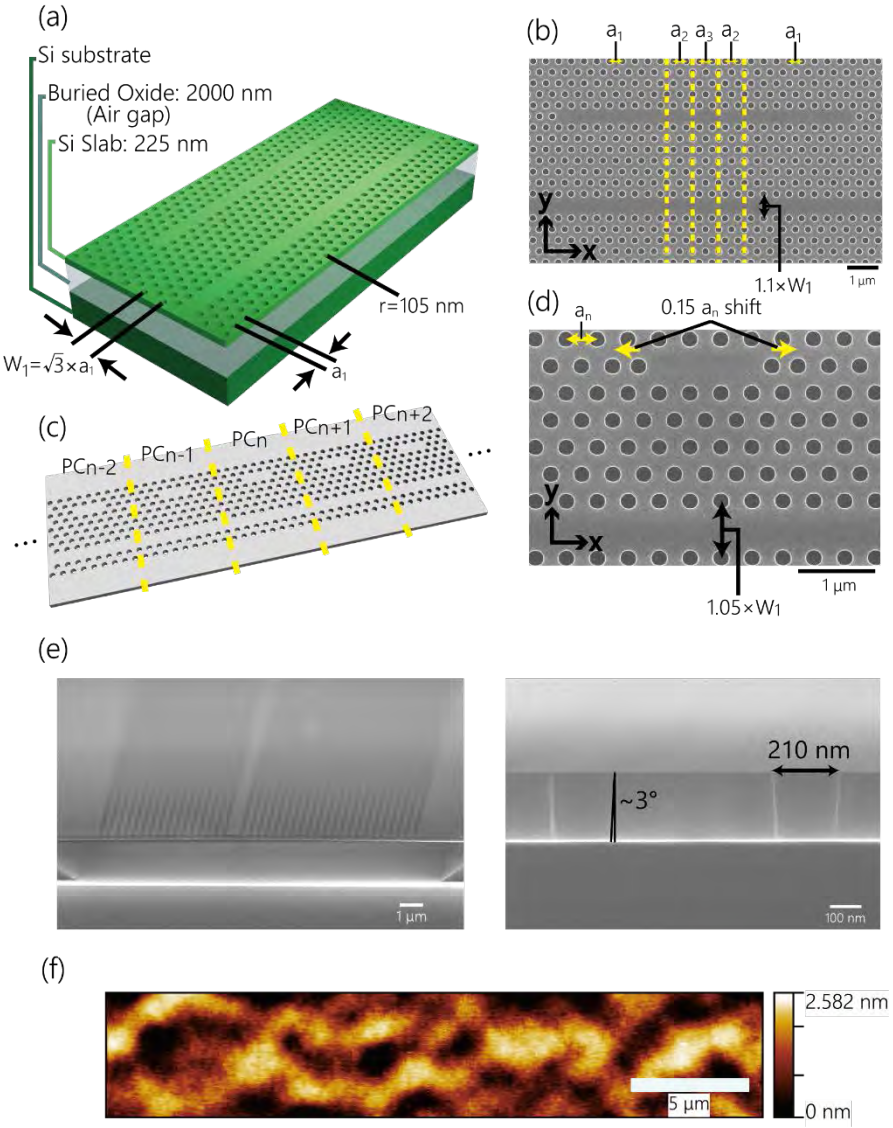

Fig. 1. Summary of fabricated samples. (a) Illustration of a measured multi-heterostructure nanocavity. (b) SEM image. (c) Illustration of a measured eight-channel drop filter consisting of arrayed L3 nanocavities. (d) SEM image of a filter unit using an L3 cavity with $0.15a_n$ shifted holes. (e) Cross-sectional SEM image of a PC slab. The magnified image indicates the tilt of the holes (about 3°). (f) AFM image of the Si surface for which Ra = 0.26 nm was obtained.

Figures 1(c) and 1(d) illustrate an eight-channel wavelength filter and SEM image of a nanocavity, respectively. This device had eight PC units (PC_1,…, PC_n,…, PC_8), and each contained an excitation waveguide and shifted L3 nanocavity to extract transmitted light with a resonant wavelength. The separation between the excitation waveguide and nanocavities was six rows of air holes. The fundamental structure was the same as that previously reported for a 32-channel drop filter fabricated with EB lithography [15]. A single PC unit had 25 periods of air holes in the *x*-direction, and the lattice constant a_n changed in the *x*-direction by

Optics EXPRESS

2 nm increments from 404 nm to 418 nm. In order to maintain structural uniformity, the lattice constant was kept the same in the *y*-direction at 710 nm for all units. The width of the excitation waveguide was $1.05W_1$. Air holes at both edges of each L3 nanocavity were shifted by $0.15a_n$. Note that the shifted air holes were completely separated from the neighboring holes, as shown in Fig. 1(d), which indicated that the proximity effect in photolithography process was very small. The calculated Q_{ideal} was 42,000, and the spacing of resonant wavelengths with an adjacent cavity was about 4.5 nm (grid frequency of 550 GHz).

The fabrication process related to the photolithography and plasma etching to form air hole structures was performed using CMOS compatible machinery in the research and development laboratory at AIST. We had to reduce the variation in air holes to less than 1 nm to realize Q_{exp} of larger than several million. Therefore, we used an ArF immersion scanner (Nikon NSR-S610C) for 45 nm node volume production. The wavelength of an ArF excimer laser is 193 nm. Purified water was introduced between the projection lens and resist-coated wafer to increase the size of the numerical aperture (N.A.) [30]. The short wavelength and large N.A. yielded a high resolution. In addition, we used a half-tone photomask to improve the resolution [31]. The shot size of the photomask was 104 mm × 132 mm; this was transferred onto a SOI wafer with a reduction in size by a factor of 4 to 26 mm × 33 mm. Thus, about 60 chips with the same structure were fabricated on a 300-mm-wide SOI. We then used a dry-etching recipe optimized for the fabrication of PC devices to reduce the tilt of the air holes.

The wafer was cut into about 60 chips and the following process was performed using our small-scale fabrication technologies. A chip was polished to a thickness of 100 μm and separated into several pieces with dimensions of 1 mm × 300 μm. They were bonded to small cubic blocks for optical measurements. Finally, the BOX layer underneath the PC pattern was selectively removed to form an air-bridge structure where 48% hydrofluoric (HF) acid without surface active agent was used at room temperature. The air-bridge structure, which easily increase the *Q* factors of nanocavities, could cause problems in CMOS process when the high-*Q* nanocavities are integrated with other opto-electronic devices. Furthermore, wet etching using HF acid is not a standard process in CMOS technologies. These can be resolved by utilizing the technologies intensively developed for MEMS, such as vapor-phase HF dry etching, trench-refill process [32, 33].

Figure 1(e) shows the cross-sectional views of a fabricated sample. The tilt of the air holes was reduced to less than 3° in average. Figure 1(f) presents an atomic force microscopy (AFM) image of the sample surface neighboring the PC pattern, which indicated an average roughness (Ra) of 0.26 nm. This value is larger than those for the nanocavities that we reported, which are typically less than 0.15 nm. This roughness was due to the 300-mm-wide SOI wafer that we used. It should not cause a significant reduction in Q_{exp} for the heterostructure nanocavities but may have increased the fluctuation of the resonant wavelengths.

3. Experimental setup

Figure 2 shows the measurement setup to obtain the resonant spectra of high-*Q* nanocavities. The light from a continuous-wave tunable laser was split into two beams. One was sent to a high-precision wavelength meter with a differential accuracy of ± 0.15 pm. The other was modulated by a mechanical chopper at a frequency of ~1 kHz and focused by a 0.40-N.A. objective lens on the facet of the excitation waveguide after being set to transverse-electric (TE) polarization by a polarizer. The experiment was performed at room temperature in a standard air atmosphere with a relative humidity of 30%. The sample was placed on a high-precision six-axis stage, and the sample temperature was stabilized by using a Peltier controller. When the incident wavelength matched λ_0 of the nanocavity, part of the transmitted light was extracted from the nanocavity in the direction perpendicular to the slab. The dropped light was collected by a 0.5-N.A. objective lens placed on a three-axis stage. The

position of the lens was adjusted by using a near-infrared (NIR) camera so that the dropped light was incident on the InGaAs photodiode. The transmitted light that passed through the excitation waveguide was similarly collected with a 0.4-N.A. objective lens. A pin hole was inserted to eliminate the background light. The intensities of the dropped and transmitted lights were measured with a lock-in amplifier system as a function of the laser wavelength.

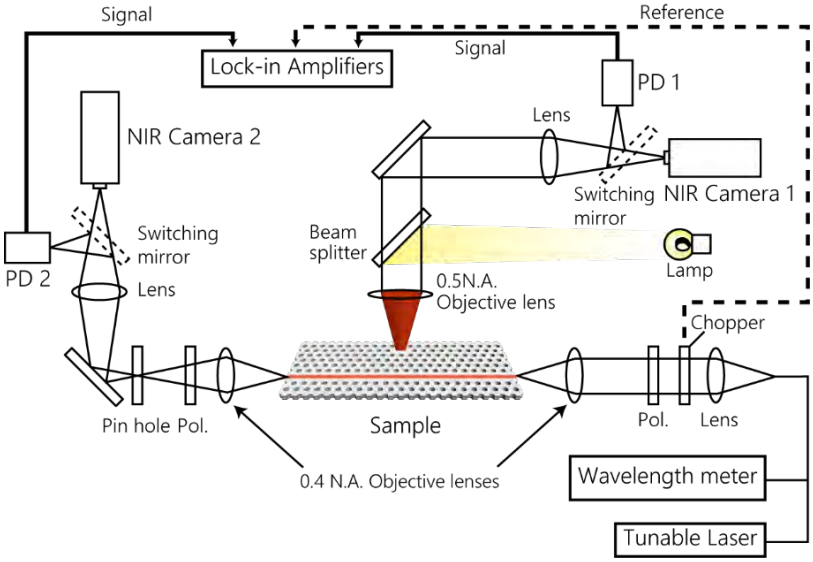

Fig. 2. Setup for measuring the resonant spectra of nanocavities. PD: photodiode, Pol.: polarizer, N.A.: numerical aperture.

4. Experimental results

4.1 Multi-heterostructure nanocavities

Among the 60 chips, we picked a chip located 50 mm away from the center of the 300-mm-wide wafer. We measured 12 samples of the multi-heterostructure nanocavity with the same structure on the chip. Figure 3 plots the dropped (filled circles) and transmitted (open circle) spectra for the heterostructure nanocavity showing the highest Q_{exp}. The dropped spectrum was fitted to a Lorentzian function (solid curved line) with a full width at half maximum ($\Delta\lambda$) of 0.82 pm. The effective Q (Q_{load}) value of the nanocavity, which included the load of the excitation waveguide, was determined according to the following relationship:

$$Q_{load} = \lambda_0 / \Delta\lambda. \quad (1)$$

Here, λ_0 is the resonant wavelength. From coupled mode theory, Q_{exp} (i.e., intrinsic Q of the measured cavity excluding the load of the excitation waveguide) can be expressed as follows [34]:

$$Q_{exp} = Q_{load} / \sqrt{T_0}. \quad (2)$$

T_0 is the transmittance at λ_0, which was 0.75 as shown in Fig. 3. Thus, a Q_{exp} value of 2.3 million was obtained for the cavity shown in Fig. 3. This value is the highest recorded for nanocavities fabricated by the CMOS process. Although the spectral measurement showed uncertainty for the sample with Q_{exp} of greater than 1 million owing to the resolution limit of the wavelength meter and temperature fluctuation, we confirmed a value of greater than 2 million from the time-domain measurement [9].

Optics EXPRESS

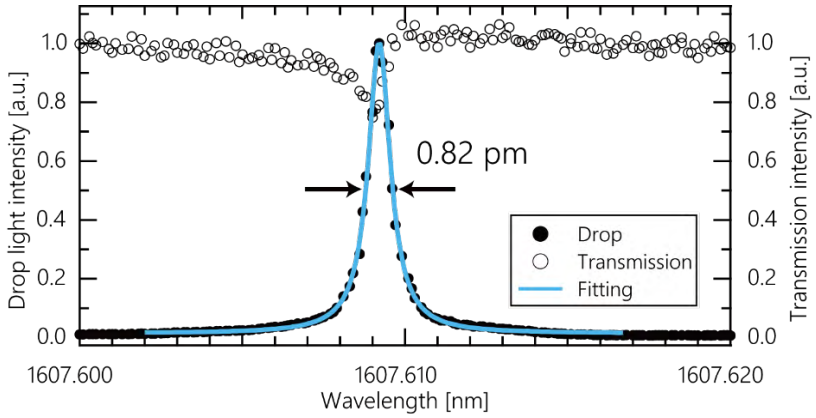

Fig. 3. Dropped (filled circles) and transmitted (open circle) spectra for the heterostructure nanocavity with the highest Q_{exp} of 2.3 million. The solid curve is the fitting by a Lorentzian function.

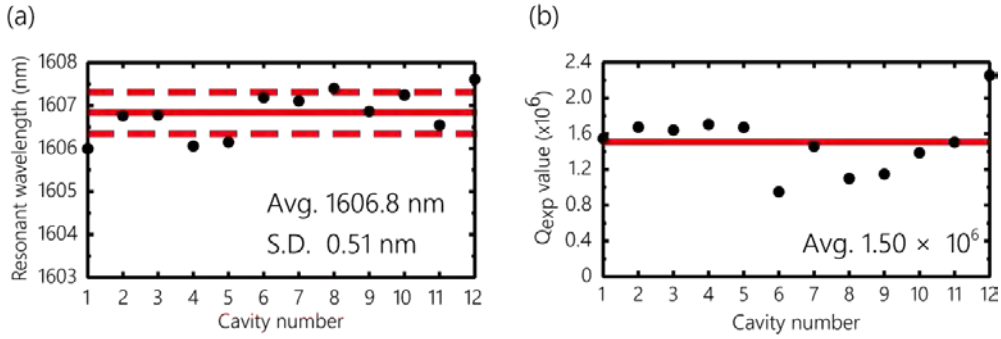

Fig. 4. (a) Resonant wavelengths and (b) experimental Q of 12 measured nanocavities. The solid and dashed lines indicate the average value and its standard deviation.

Figures 4(a) and 4(b) summarize λ_0 and Q_{exp}, respectively, for the measured 12 nanocavities. The x-axis represents the number of the cavities. The average λ_0 was 1606.8 nm, which is in good agreement with the calculated value. The standard deviation of the resonant wavelength was as small as 0.51 nm. The solid line in Fig. 4(b) indicates the average Q_{exp} value of the 12 nanocavities, which was as high as 1.50×10^6. This value is much smaller than Q_{ideal} because of scattering loss from random variation of the air holes and optical absorption loss related to the surface [12]. We obtained similar results for Q_{exp} and the standard deviation of λ with a chip picked from another position on the 300-mm-wide SOI (the average λ varied in several nanometers, which will be reported elsewhere). These results clearly indicate that the mass manufacture of ultrahigh-Q nanocavities with Q_{exp} of greater than 1 million is feasible by using CMOS-compatible technologies. We expect that the mass manufacture of a nanocavity Raman silicon laser would be possible with the CMOS process [23]. Note that the tilt of the air holes in this study was greater than that in previous studies using EB lithography [10–12]. In addition, the thickness of the BOX layer for the SOI was 2 μm in this study, while previous studies utilized an SOI with a 3-μm-thick BOX layer. The tilt of the air holes increases the scattering loss, and a thin BOX layer increases the radiation loss in the direction toward the substrate. By improving upon these two points, we can increase Q_{exp} for CMOS fabrication.

4.2 Estimation of air hole variation

Q_{exp} for CMOS fabrication was less than that for EB lithography. This must mainly be due to the larger variation of the air holes with CMOS fabrication. To further increase Q_{exp}, we

should know the magnitude of the random variation of the air holes, which is represented by the standard deviation σ_{hole}. As we previously reported, the magnitude of σ_{hole} was estimated from the comparison with 3D FDTD simulations considering air hole variations [10, 12, 26]. In this calculation, random nanometer-scale variations in the positions (δx, δy) and radii (δr) were applied to all air holes so that the probability of variations followed a normal distribution with a standard deviation. The size of a unit cell in 3D FDTD was set to the one-twentieth of the lattice constant in the x and y directions, which is twice as small as that of the previous report [10]. The smaller unit cell enhanced the accuracy of the simulation, especially for λ. The calculated Q (Q_{fluc}) values were strongly dependent on the fluctuation pattern. Thus, we performed the calculation for 30 different fluctuation patterns.

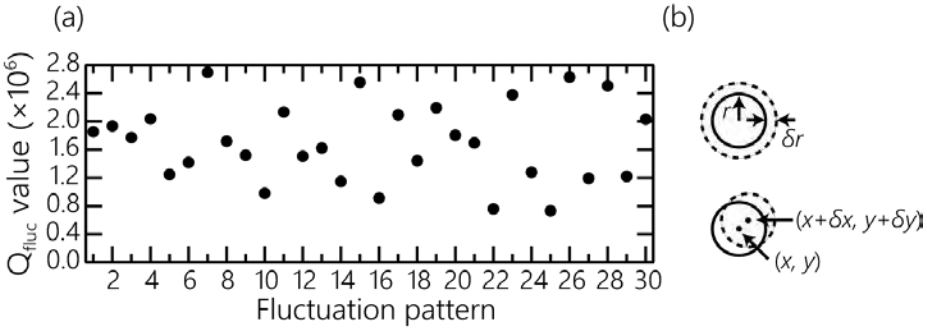

Fig. 5. (a) Calculated Q factors of the nanocavity shown in Fig. 1(b) for 30 fluctuation patterns with σ_{hole} = 1 nm. (b) Schematic view of the variation in an air hole's radius and position. δx and δy represent the variation in position. δr represents the variation in radius.

Figure 5 shows the Q_{fluc} values for the 30 patterns with σ_{hole} of 1 nm (standard deviations for δr, δx, and δy are 1 nm). These were less than $Q_{ideal} = 2.12 \times 10^7$ because of the additional loss factor (Q_{loss}) from the air hole variations. The three Q had the following relation:

$$1/Q_{loss} = 1/Q_{fluc} - 1/Q_{ideal}. \quad (3)$$

This statistical simulation yielded the following relations for the average value (Avg.) of $1/Q_{loss}$ and the standard deviation (S.D.) of $1/Q_{loss}$ because they are proportional to the square of σ_{hole} (details of the calculations are given in [26]):

$$\text{Avg.}(1/Q_{loss}) = 6.17 \times 10^{-7} \times \sigma_{hole}^2. \quad (4)$$

$$\text{S.D.}(1/Q_{loss}) = 2.57 \times 10^{-7} \times \sigma_{hole}^2. \quad (5)$$

These coefficients of 6.17×10^{-7} and 2.57×10^{-7} are smaller than those for our previous reports on nanocavities with a similar structure [10, 12]. We confirmed that the smaller radius decreases the coefficients for the same magnitude of σ_{hole} because the refractive index variation induced by the air hole fluctuation is decreased. Avg.($1/Q_{loss}$) and S.D.($1/Q_{loss}$) for the 12 nanocavities shown in Fig. 4(b) were estimated to be 6.52×10^{-7} and 1.61×10^{-7}, respectively, by the substitution of Q_{exp} for Q_{fluc} in Eq. (3). The experimental Avg.($1/Q_{loss}$) should include the absorption loss related to the nanocavity surface [12,14], which was estimated to be about 1.25×10^{-7} (Q_{loss} = 8 million) for the sample in this study. The magnitude of the air hole variations for CMOS fabrication was estimated to be σ_{hole} = 0.92 nm by substituting 5.27×10^{-7} for the Avg.($1/Q_{loss}$) in Eq. (4) while σ_{hole} = 0.79 nm was estimated by substituting 1.61×10^{-7} for the S.D.($1/Q_{loss}$) in Eq. (5).

In addition, the simulation yielded the following relation for the S.D. of λ, which is known to be proportional to σ_{hole}.

$$\text{S.D.}(\lambda) = 0.63 \times \sigma_{hole}. \quad (6)$$

The coefficient of 0.63 is larger than that for the previous report [10]. This is probably because of the smaller sizes of the unit cell in 3D FDTD. σ_{hole} was estimated to be 0.81 nm from Eq. (6) by substituting the experimental result of 0.51 nm for the S.D.(λ). The good agreement between σ_{hole} estimated from λ and the values estimated from the $1/Q_{loss}$ suggests that the surface roughness shown in Fig. 1(f) may not have a large influence on λ. The three values of σ_{hole} estimated from the three methods mostly showed good agreement with an average σ_{hole} of 0.84 nm. The lowest value of σ_{hole} for EB fabrication was 0.25 nm, for which the highest Q_{exp} of 11 million was reported [14]. We expect σ_{hole} for CMOS fabrication to be further decreased as the accuracy of the photomask can be improved and the photolithography conditions will be optimized.

4.3 Add-drop filter

Finally, we demonstrate an eight-channel drop filter using arrayed L3 nanocavities for the wavelength division multiplexing (WDM) applications. The demultiplexing (DEMUX) filter using Si photonics is an important component for future optical links in huge datacenters. The size of a DEMUX filter using high-Q nanocavities is much smaller than other types of silicon photonics filters such as arrayed waveguide gratings or ring cavities [35, 36]. Recently, an eight-channel DEMUX filter with integrated heaters using photonic crystal nanocavities has been reported [37]. Figure 6(a) shows the drop spectra for eight channels in the sample showing the smallest fluctuation of the λ spacing. Each spectrum was normalized independently. The average value of Q_{load} for the eight channels was 3.13×10^4. Figure 6(b) shows the relation between the measured drop wavelengths and the lattice constant in the x-direction. The resonant wavelengths were proportional to the lattice constant. The slope of the fitted line indicated that the resonant wavelength changed by 3.9 nm when the lattice constant was increased by 2 nm. This value corresponds to a spacing of 460 GHz, which is smaller than the calculated value. This is possibly due to an error in the photomask. The variation in spacing of resonant wavelengths for neighboring nanocavities had a standard deviation of as small as 0.41 nm, which would be negligible when applied to coarse WDM. For future applications, it is important to study increasing the 1 dB bandwidth [38].

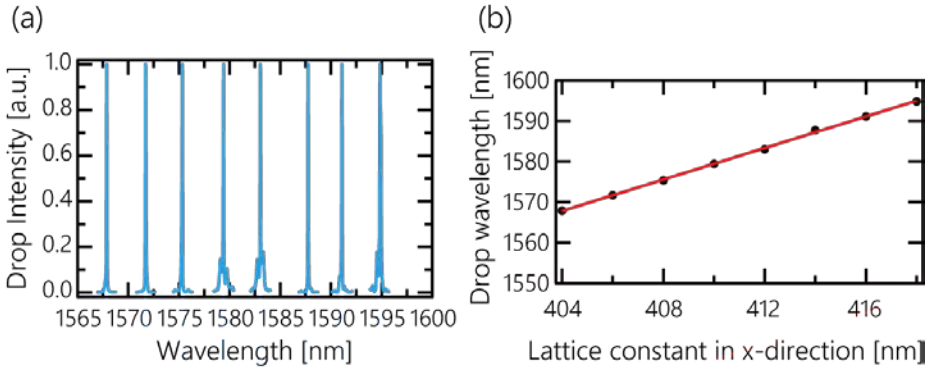

Fig. 6. (a) Normalized drop spectra for eight channels (b) Relationship between the drop wavelength and lattice constant in the x direction for an eight-channel filter. The red line shows a linear fit.

The 3D FDTD simulation (see section 4.2) for the shifted L3 nanocavity with a = 410 nm and r = 105 nm yielded the following relation for the S.D. of λ:

$$\text{S.D.}(\lambda) = 0.68 \times \sigma_{hole}. \quad (7)$$

The coefficient is slightly larger than that for the heterostructure nanocavity represented in Eq. (6). This suggests that the L3 cavities have a slightly lower tolerance to random structural disorders.

Optics EXPRESS

5. Summary

Nanocavities fabricated on a 300-mm-wide SOI using ArF immersion photolithography showed good properties in terms of the magnitude of Q_{exp} and accuracy of the resonant wavelengths. The heterostructure nanocavities showed an average Q_{exp} value of 1.5 million for 12 measured samples. The highest Q_{exp} value was 2.3 million, which represents a record for PC cavities fabricated by a CMOS-compatible process. We also demonstrated an eight-channel drop filter with 460 GHz spacing consisting of arrayed L3 nanocavities where the variation in drop wavelengths was less than 1 nm. The Q_{exp} values will soon be enhanced because we can further improve upon the device structures and the CMOS fabrication process. We believe that a nanocavity Raman silicon laser can be realized with the CMOS process [23]. Such results will accelerate high-Q nanocavity research for applications in various areas.

Funding

JSPS KAKENHI (15H05428, 15K13326); Toray Science Foundation; Asahi Grass Foundation; Support Center for Advanced Telecommunications Technology Research Foundation; New Energy and Industrial Technology Development Organization (NEDO).

Acknowledgment

K. Ashida was supported by a fellowship from ICOM Electronic Communication Engineering Promotion Foundation. The AFM measurement in this work was supported by Kyoto University Nano Technology Hub in “Nanotechnology Platform Project” sponsored by the Ministry of Education, Culture, Sports, Science and Technology (MEXT), Japan.